

Sussex Research

Pseudopeptidic ligands: exploring the self-assembly of isophthaloylbisglycine (H2IBG) and divalent metal ions

Vasiliki N Dokorou, Constantinos J Milios, Athanassios C Tsipis, Matti Haukka, Peter G Weidler, Annie K Powell, George Kostakis

Publication date

01-01-2012

Licence

This work is made available under the **Copyright not evaluated** licence and should only be used in accordance with that licence. For more information on the specific terms, consult the repository record for this item.

Citation for this work (American Psychological Association 7th edition)

Dokorou, V. N., Milios, C. J., Tsipis, A. C., Haukka, M., Weidler, P. G., Powell, A. K., & Kostakis, G. (2012). *Pseudopeptidic ligands: exploring the self-assembly of isophthaloylbisglycine (H2IBG) and divalent metal ions* (Version 1). University of Sussex. <https://hdl.handle.net/10779/uos.23399081.v1>

Published in

Dalton Transactions

Link to external publisher version

<https://doi.org/10.1039/c2dt31383a>

Copyright and reuse:

This work was downloaded from Sussex Research Open (SRO). This document is made available in line with publisher policy and may differ from the published version. Please cite the published version where possible. Copyright and all moral rights to the version of the paper presented here belong to the individual author(s) and/or other copyright owners unless otherwise stated. For more information on this work, SRO or to report an issue, you can contact the repository administrators at sro@sussex.ac.uk. Discover more of the University's research at <https://sussex.figshare.com/>

Pseudopeptidic ligands: exploring the self-assembly of isophthaloylbisglycine (H2IBG) and divalent metal ions

Article (Unspecified)

Citation:

Dokorou, Vasiliki N, Milios, Constantinos J, Tsipis, Athanassios C, Haukka, Matti, Weidler, Peter G, Powell, Annie K and Kostakis, George E (2012) Pseudopeptidic ligands: exploring the self-assembly of isophthaloylbisglycine (H2IBG) and divalent metal ions. Dalton Transactions, 41. pp. 12501-12513. ISSN 1477-9226

This version is available from Sussex Research Online: <http://sro.sussex.ac.uk/46681/>

This document is made available in accordance with publisher policies and may differ from the published version or from the version of record. If you wish to cite this item you are advised to consult the publisher's version. Please see the URL above for details on accessing the published version.

Copyright and reuse:

Sussex Research Online is a digital repository of the research output of the University.

Copyright and all moral rights to the version of the paper presented here belong to the individual author(s) and/or other copyright owners. To the extent reasonable and practicable, the material made available in SRO has been checked for eligibility before being made available.

Copies of full text items generally can be reproduced, displayed or performed and given to third parties in any format or medium for personal research or study, educational, or not-for-profit purposes without prior permission or charge, provided that the authors, title and full bibliographic details are credited, a hyperlink and/or URL is given for the original metadata page and the content is not changed in any way.

Cite this: *Dalton Trans.*, 2012, **41**, 12501

www.rsc.org/dalton

PAPER

Pseudopeptidic ligands: exploring the self-assembly of isophthaloylbisglycine (H₂IBG) and divalent metal ions†Vassiliki N. Dokorou,^{a,b} Constantinos J. Milios,^c Athanassios C. Tsipis,^d Matti Haukka,^e Peter G. Weidler,^f Annie K. Powell^{a,g} and George E. Kostakis^{*a}

Received 27th June 2012, Accepted 10th August 2012

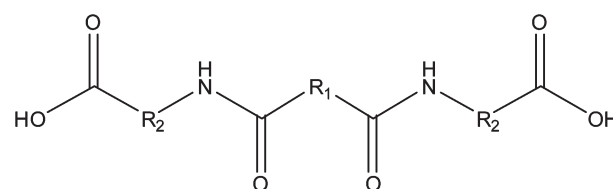
DOI: 10.1039/c2dt31383a

We present a systematic study of the complexation of the new pseudopeptidic ligand isophthaloylbisglycine (H₂IBG) with divalent metal ions of varying ionic radius. This work represents the initial employment of H₂IBG in the coordination chemistry of alkaline earth, 3d transition, Zn(II) and Cd(II) metal elements. Infrared, NMR, thermal, magnetic, adsorption and theoretical studies of these compounds are also discussed.

Introduction

In recent years, a number of basic inorganic principles have provided the framework and inspiration for chemists in developing coordination chemistry with a view to synthesizing materials with potential applications.¹ For example, peptides coordinating transition metal elements have been used to obtain “bioinspired” microporous coordination polymers with an emphasis on catalysis.² In addition, coordination polymers based on amino acid backbones have gained widespread interest due to their intriguing properties such as asymmetric catalysis, chiral sorption, etc.³

A pseudopeptidic ligand can be described as a molecule belonging to the class of compounds where amino acids or oligo-peptides are attached to scaffolds which may be aromatic or non-aromatic. Several research groups are using various types of pseudopeptidic ligands for the synthesis of macrocycles or coordination polymers.^{4–6} Up to now, we have focused on the investigation of the coordination abilities of a specific type of pseudopeptidic ligand drawn in Scheme 1, for the synthesis of



Scheme 1 The general motif of the pseudopeptidic ligand.

zero or multidimensional compounds.⁶ These multidentate ligands have a semi- or fully flexible backbone offering several positions for coordination and hydrogen bonding interactions. These are important features since the nature of the amino acid or oligo-peptide (R₂, Scheme 1) and that of the scaffold (R₁, Scheme 1) can vary the solubility and the coordination abilities of the ligand. In this way, the introduction of different R groups (R₁ or R₂, Scheme 1) allows for the possibility, for example, of obtaining chiral compounds or water-friendly “green” nanoporous products easily, suggesting that pseudopeptidic ligands represent a class of compounds which deserve attention.

Up to now, we have studied the complexation abilities of terephthaloylbisglycinate (TBG²⁻, R₁ = *p*-C₆H₄, R₂ = CH₂, Scheme 1) with metal ions at room temperature which resulted in the formation of infinite non-porous coordination polymers with fascinating topologies.^{6a,c} Furthermore, it was found that the compound [Cu(TBG)(μ-H₂O)(H₂O)₂]₂·2(H₂O) represents an efficient heterogeneous catalyst for the oxidation of 3,5-di-*tert*-butylcatechol (DTBC), and where the Cu–Cu distance of ca. 4 Å, similar to that found in tyrosinase, may be an important factor. The next logical step in our study was to extend the flexible arms of the H₂TBG ligand by one methylene group and thus we studied the complexation abilities of terephthaloyl-bis-β-alaninate (TBbA²⁻, R₁ = *p*-C₆H₄, R₂ = CH₂CH₂, Scheme 1) with metal ions at room temperature which resulted in the isolation of polymeric compounds with interesting topological and crystal engineering features.^{6d} As an extension of this project, we present herein our investigation on the influence of

^aInstitute of Nanotechnology, Karlsruhe Institute of Technology, Hermann-von-Helmholtz Platz 1, 76344 Eggenstein-Leopoldshafen, Germany. E-mail: george.kostakis@kit.edu

^bX-Ray Unit, Department of Chemistry, University of Ioannina, 45110 Ioannina, Greece

^cDepartment of Chemistry, The University of Crete, Voutes, 71003, Herakleion, Greece

^dLaboratory of Inorganic and General Chemistry, Department of Chemistry, University of Ioannina, 451 10 Ioannina, Greece

^eUniversity of Jyväskylä, Department of Chemistry, P.O. Box 35, FI-40014 University of Jyväskylä, Finland

^fInstitute of Functional Interfaces, Karlsruhe Institute of Technology, Hermann-von-Helmholtz Platz 1, 76344 Eggenstein-Leopoldshafen, Germany

^gInstitute of Inorganic Chemistry, Karlsruhe Institute of Technology, Engesserstrasse 15, 76131 Karlsruhe, Germany

†Electronic supplementary information (ESI) available: Fig. S1–S13. CCDC 886200–886207. For ESI and crystallographic data in CIF or other electronic format see DOI: 10.1039/c2dt31383a

substituents on the aromatic ring. Thus, we have chosen to synthesize the new pseudopeptidic ligand isophthaloylbisglycine (H_2IBG , $\text{R}_1 = m\text{-C}_6\text{H}_4$, $\text{R}_2 = \text{CH}_2$, Scheme 1) (**1**). A further motivation for this work was that whilst 3d transition metal elements⁷ have been widely used for the synthesis of multi-dimensional coordination polymers the use of alkaline earth elements is much rarer⁸ and we thought it of interest to compare the coordination behaviour of these two classes of compounds, especially given the important role of alkaline earths in bio-inorganic chemistry.

Thus, nine new compounds formulated as $[\text{Mg}(\text{H}_2\text{O})_6][\text{IBG}]\cdot 5.5(\text{H}_2\text{O})$ (**2**), $[\text{Ca}(\text{IBG})(\text{H}_2\text{O})_2]$ (**3**), $[\text{Sr}(\text{IBG})(\text{H}_2\text{O})_3]\cdot 2(\text{H}_2\text{O})$ (**4**), $[\text{Mn}(\text{IBG})(\text{H}_2\text{O})_4]\cdot 2(\text{H}_2\text{O})$ (**5**), $[\text{Co}(\text{IBG})(\mu\text{-H}_2\text{O})(\text{H}_2\text{O})_2]\cdot 2(\text{H}_2\text{O})$ (**6**), $[\text{Ni}(\text{IBG})(\mu\text{-H}_2\text{O})(\text{H}_2\text{O})_2]\cdot 2(\text{H}_2\text{O})$ (**7**), $[\text{Cu}(\text{IBG})(\mu\text{-H}_2\text{O})(\text{H}_2\text{O})_2]\cdot 2(\text{H}_2\text{O})$ (**8**), $[\text{Zn}(\text{IBG})(\text{H}_2\text{O})_3]\cdot 2(\text{H}_2\text{O})$ (**9**), $[\text{Cd}(\text{IBG})(\text{H}_2\text{O})_3]\cdot 2(\text{H}_2\text{O})$ (**10**) have been synthesized and characterized by elemental analysis, IR spectroscopy, powder X-ray diffraction and single-crystal X-ray diffraction measurements. Infrared, NMR, thermal, magnetic, adsorption and theoretical studies of those compounds are also discussed.

Experimental

Materials and methods

All chemicals and solvents used for synthesis were obtained from commercial sources and used as received without further purification. All reactions were carried out under aerobic conditions. The ^1H -NMR and ^{13}C -NMR spectra were recorded on a Bruker AMX 500 MHz spectrometer. All spectra were recorded using commercially available $\text{d}_6\text{-DMSO}$ or D_2O (Aldrich) of 99.6% isotopic purity or better and referenced to a residual solvent. The elemental analyses (C, H and N) were carried out at the Institute of Nanotechnology, Karlsruhe Institute of Technology, using an Elementar Vario EL analyzer. Fourier transform IR spectra (4000 to 400 cm^{-1}) were measured on a Perkin-Elmer Spectrum GX spectrometer with samples prepared as KBr discs. UV-Vis diffuse reflectance spectra (DRS) of **6** and its dehydrated and rehydrated analogues were recorded on a Perkin-Elmer UV/vis/NIR Lambda 900 spectrophotometer. Variable-temperature, solid-state direct current (dc) magnetic susceptibility data down to 5 K were collected on a Quantum Design MPMS-XL SQUID magnetometer (University of Crete) equipped with a 7 T dc magnet. Diamagnetic corrections were applied to the observed paramagnetic susceptibilities using Pascal's constants.

Synthetic part

Synthesis of isophthaloyl-bis- β -glycine (IBGH₂) (1). Glycine (6.006 g, 0.080 mol) and NaOH (4.80 g, 0.120 mol) were dissolved in water (50 mL) with stirring in a round-bottom flask in an ice bath. After the solution cooled to below 10°C , a solution of isophthaloylchloride (8.12 g, 0.040 mol) dissolved in toluene (50 mL) was added dropwise. The reaction mixture was stirred for one hour, after which the aqueous phase was separated from the organic phase and collected. The aqueous phase was acidified with 35% HCl until the pH was approximately 1. The white product was collected by vacuum filtration and dried in a vacuum oven overnight at 50°C . Yield: 11.84 g, 100%. Anal.

calcd for $\text{C}_{12}\text{H}_{12}\text{N}_2\text{O}_6$ (found): C, 51.43 (51.22); H, 4.32 (4.20); N, 9.99 (9.80)%. ^1H -NMR (ppm): 3.96 (d, 4H, $J = 5.8\text{ Hz}$), 7.61 (t, 1H, $J = 7.8\text{ Hz}$), 8.02 (dd, 2H, $J_1 = 7.8$, $J_2 = 1.70$), 8.38 (s, 1H), 8.97 (t, 2H, $J = 5.90\text{ Hz}$), 12.68 (s, 2H). ^{13}C -NMR (ppm): 41.24, 126.42, 128.52, 129.95, 134.09, 166.02, 171.20. Selected IR data (KBr disc, cm^{-1}): 3287, 3063, 2976, 2867, 2560, 1713, 1643, 1536, 1434, 1408, 1340, 1325, 1295, 1269, 1243, 1072, 1026, 1002, 919, 895, 819, 738, 673, 644.

Synthesis of $[\text{Mg}(\text{H}_2\text{O})_6][\text{IBG}]\cdot 5.5(\text{H}_2\text{O})$ (2). The same procedure was followed for the preparation of all compounds, so only the synthesis of **2** is described in detail. H_2IBG (140 mg, 0.500 mmol) and K_2CO_3 (69 mg, 0.500 mmol) were dissolved in water (25 mL) with stirring. $\text{Mg}(\text{NO}_3)_2\cdot 3\text{H}_2\text{O}$ (128 mg, 0.500 mmol) was added to the solution. The solution was stirred at room temperature for five minutes and then filtered and left undisturbed. Slow evaporation yielded colourless crystals after almost 2 months. The crystals were collected by filtration and washed with water. Yield: 215 mg, 85% based on Mg. Anal. calcd for $\text{C}_{24}\text{H}_{66}\text{Mg}_2\text{N}_4\text{O}_{35}$ (found): C, 28.27 (28.03); H, 6.52 (6.78); N, 5.50 (5.79)%. Selected IR data (KBr disc, cm^{-1}): 3325, 2937, 2400, 1632, 1579, 1544, 1445, 1399, 1303, 1280, 1090, 1065, 1021, 1003, 936, 912, 824, 745, 686.

Synthesis of $[\text{Ca}(\text{IBG})(\text{H}_2\text{O})_2]$ (3). The metal salt used was $\text{Ca}(\text{NO}_3)_2\cdot 4\text{H}_2\text{O}$. The product was obtained as colourless needles. Yield: 129 mg, 73% based on Ca. Anal. calcd for $\text{C}_{12}\text{H}_{14}\text{CaN}_2\text{O}_8$ (found): C, 40.67 (40.43); H, 3.98 (3.99); N, 7.90 (7.86)%. Selected IR data (KBr disc, cm^{-1}): 3533, 3398, 3268, 1633, 1598, 1573, 1481, 1437, 1396, 1336, 1299, 1280, 1247, 1191, 1076, 1021, 1001, 949, 928, 821, 737, 690, 659, 629.

Synthesis of $[\text{Sr}(\text{IBG})(\text{H}_2\text{O})_3]\cdot 2(\text{H}_2\text{O})$ (4). The metal salt used was $\text{Sr}(\text{NO}_3)_2\cdot 6\text{H}_2\text{O}$. The product was obtained as colourless needles. Yield: 201 mg, 88% based on Sr. Anal. calcd for $\text{C}_{12}\text{H}_{20}\text{N}_2\text{O}_{11}\text{Sr}$ (found): C, 31.61 (31.83); H, 4.42 (4.27); N, 6.14 (6.23)%. Selected IR data (KBr disc, cm^{-1}): 3401, 1646, 1576, 1478, 1435, 1400, 1315, 1298, 1020, 931, 814, 748, 721.

Synthesis of $[\text{Mn}(\text{IBG})(\text{H}_2\text{O})_4]\cdot 2(\text{H}_2\text{O})$ (5). The metal salt used was $\text{Mn}(\text{OAc})_2\cdot 4\text{H}_2\text{O}$. The product was obtained as colourless needles. Yield: 129 mg, 62% based on Mn. Anal. calcd for $\text{C}_{14}\text{H}_{20}\text{MnN}_2\text{O}_9$ (found): C, 40.49 (40.63); H, 4.86 (4.67); N, 6.74 (6.73)%. Selected IR data (KBr disc, cm^{-1}): 3333, 1634, 1580, 1544, 1439, 1395, 1302, 1280, 1063, 1020, 1002, 911, 822, 741, 685.

Synthesis of $[\text{Co}(\text{IBG})(\mu\text{-H}_2\text{O})(\text{H}_2\text{O})_2]\cdot 2(\text{H}_2\text{O})$ (6). The metal salt used was $\text{Co}(\text{NO}_3)_2\cdot 6\text{H}_2\text{O}$. The product was obtained as colourless needles. Yield: 171 mg, 80% based on Co. Anal. calcd for $\text{C}_{12}\text{H}_{20}\text{CoN}_2\text{O}_{11}$ (found): C, 33.74 (33.20); H, 4.71 (4.76); N, 6.56 (6.40)%. Selected IR data (KBr disc, cm^{-1}): 3350, 2961, 2927, 1651, 1564, 1483, 1439, 1406, 1323, 1267, 1196, 1069, 982, 907, 746, 693.

Synthesis of $[\text{Ni}(\text{IBG})(\mu\text{-H}_2\text{O})(\text{H}_2\text{O})_2]\cdot 2(\text{H}_2\text{O})$ (7). The metal salt used was $\text{Ni}(\text{NO}_3)_2\cdot 6\text{H}_2\text{O}$. The product was obtained as colourless needles. Yield: 173 mg, 81% based on Ni. Anal. calcd for $\text{C}_{12}\text{H}_{20}\text{CoN}_2\text{O}_{11}$ (found): C, 33.75 (33.12); H, 4.72 (4.76); N, 6.56 (6.40)%. Selected IR data (KBr disc, cm^{-1}): 3343, 2963,

2928, 2248, 1653, 1563, 1483, 1441, 1408, 1325, 1303, 1267, 1195, 1135, 1068, 1009, 916, 834, 746, 692.

Synthesis of [Cu(IBG)(μ -H₂O)(H₂O)₂] \cdot 2(H₂O) (8**).** The metal salt used was Cu(NO₃)₂ \cdot 3H₂O. The product was obtained as colourless needles. Yield: 162 mg, 75% based on Cu. Anal. calcd for C₁₂H₂₀CuN₂O₁₁ (found): C, 33.38 (33.22); H, 4.69 (4.46); N, 6.49 (6.40)%. Selected IR data (KBr disc, cm⁻¹): 3364, 2928, 1654, 1586, 1561, 1482, 1431, 1397, 1385, 1313, 1263, 1197, 1068, 1009, 924, 746, 717, 689.

Synthesis of [Zn(IBG)(H₂O)₃] \cdot 2(H₂O) (9**).** The metal salt used was Zn(NO₃)₂ \cdot 4H₂O. The product was obtained as colourless needles. Yield: 141 mg, 65% based on Zn. Anal. calcd for C₁₂H₂₀N₂O₁₁Zn (found): C, 33.23 (33.03); H, 4.65 (4.47); N, 6.46 (6.33)%. Selected IR data (KBr disc, cm⁻¹): 3348.35, 1630, 1590, 1544, 1478, 1438, 1397, 1307, 1260, 1002, 929, 824, 688.

Synthesis of [Cd(IBG)(H₂O)₃] \cdot 2(H₂O) (10**).** The metal salt used was Cd(NO₃)₂ \cdot 4H₂O. The product was obtained as colourless needles. Yield: 180 mg, 75% based on Cd. Anal. calcd for C₁₂H₂₀CdN₂O₁₁ (found): C, 29.99 (30.23); H, 4.19 (4.07); N, 5.83 (5.73)%. Selected IR data (KBr disc, cm⁻¹): 3348.35, 1630, 1590, 1544, 1478, 1438, 1397, 1307, 1260, 1002, 929, 824, 688.

Thermal studies

Thermogravimetric analysis (TGA) curves were measured using a Netzsch STA 409C Thermal Analyzer under nitrogen flow (30 mL min⁻¹) at a scan rate of 5 °C min⁻¹ from 25 to 800 °C. The reversibility of water loss of compounds **6**, **7** and **8** was confirmed by heating a small sample of each in a vacuum oven at 50 °C overnight. The dehydrated product was characterized by IR, powder XRD, UV/Vis DRS and elemental analysis. The dehydrated product was then rehydrated by suspending the sample in water. The dehydration/rehydration procedure was repeated on the same sample and characterized by IR to confirm that the water loss is reversible.

Computational details

All calculations were performed using the Gaussian03 suite of programs⁹ employing the recently developed DSD-PBEP86 (including spin-component scaled MP2 and dispersion corrections)^{10a} functional combined with the Def2-TZVP basis set,^{10b} for the model complexes chosen and the nonlocal hybrid generalized gradient approximation (GGA) PBE0,^{10c-h} combined with the Pople's 6-311+G(d,p) basis set for the H₂IBG and IBG²⁻ ligands. Full geometry optimization was performed for each structure using Schlegel's analytical gradient method¹⁰ⁱ and the attainment of the energy minimum was verified by calculating the vibrational frequencies that result in the absence of imaginary eigenvalues. The harmonic vibrational frequencies were scaled employing the fundamental vibration frequency scale factor 0.9594.^{10j} This was achieved with the SCF convergence on the density matrix of at least 10⁻⁹ and the rms force less than 10⁻⁴ au. All bond lengths and bond angles were optimized to

better than 0.001 Å and 0.1°, respectively. The computed electronic energies were corrected for zero point energy (ZPE) differences. ¹H and ¹³C NMR shielding tensors have been computed with the GIAO (gauge-including atomic orbitals) DFT method^{10k,l} as implemented in the GAUSSIAN03 series of programs⁹ employing the PBE0 functional. The potential energy surfaces for the adiabatic rotation of the glycine ligand around the M–O (M = Mn, Cu) bond were calculated at the DSD-PBEP86/Def2-TZVP level of theory. The reduced density gradient (RDG) plots were obtained employing the Multiwfn software version 2.2.1.^{10m}

Single crystal X-ray data collection and structure determination

Data for **1–10** were collected at 180 K on a Stoe IPDS II area detector diffractometer using graphite-monochromated Mo-K α radiation. Semi-empirical absorption corrections were applied using *XPREP* in *SHELXTL*.¹¹ The structures were solved using direct methods, followed by a full-matrix least-squares refinement against *F*² (all data) using *SHELXTL*.¹¹ Anisotropic refinement was used for all ordered non-hydrogen atoms; organic hydrogen atoms were placed in calculated positions, while coordinates of hydroxo hydrogen and amine hydrogen atoms were either placed in calculated positions or located from the difference Fourier map and then constrained to ride on their parent atom with *U*_{iso} = 1.5*U*_{eq}(parent atom). The crystallographic and structure refinement data for all compounds are given in Table 1. The crystals of **4** and **8** were refined as a twin using the twin matrix [1 0 0.147 0 -1 0 0 0 -1] and [1 0 0.140 0 -1 0 0 0 -1] and the BASF were refined to 0.12164, 0.26067, respectively. The crystal structure of **5** was a solved monoclinic *Cc* space group. All efforts to solve this structure in a higher symmetry space group such as *Ama*2 suggested by Platon were proved impossible. CCDC 886200–886207.

Results

Synthesis

All compounds were prepared under normal atmospheric conditions in aqueous solutions. Isomorphous compounds were obtained using several bases such as sodium carbonate, lithium hydroxide, or sodium hydroxide instead of potassium carbonate. Using different metal salts including nitrate, chloride, acetate, and sulphate did not result in any change to the motif of the final products. Besides, reactions with an excess either of the metal salt or the ligand, with different metal-to-ligand ratios (3 : 1 to 1 : 3), also result in the formation of the same isomorphous products demonstrating the stability of the compounds which also retain their crystallinity on exposure to air. The phase purity of the products arising from all the employed reaction conditions was checked for all compounds by comparing their powder XRD patterns with those simulated from the single crystal studies (see Fig. S1–S6†).

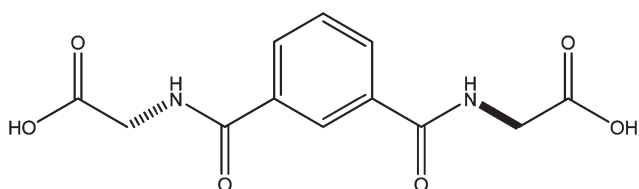
Ligand conformation

Before going into a detailed description of the crystal structures, it is important to establish a nomenclature in order to clarify the

Table 1 Crystallographic and structure refinement data for compounds **1–10**

	1	2	3	4	5
Formula	C ₁₂ H ₁₂ N ₂ O ₆	C ₂₄ H ₆₄ Mg ₂ N ₄ O ₃₅	C ₁₂ H ₁₄ CaN ₂ O ₈	C ₁₂ H ₂₀ N ₂ O ₁₁ Sr	C ₁₂ H ₁₈ MnN ₂ O ₁₂
<i>M_r</i>	280.24	1017.41	354.33	455.92	437.22
Crystal system	Monoclinic	Triclinic	Monoclinic	Monoclinic	Monoclinic
Space group	<i>C2/c</i>	<i>P1</i>	<i>C2/m</i>	<i>P2/c</i>	<i>Cc</i>
<i>T</i> (K)	180(2)	180(2)	180(2)	180(2)	200(2)
<i>a</i> (Å)	6.4778(14)	7.2573(10)	6.6529(11)	15.246(3)	6.9305(12)
<i>b</i> (Å)	7.3896(11)	12.1847(16)	25.696(6)	6.8008(9)	7.8963(13)
<i>c</i> (Å)	26.049(5)	14.7493(18)	8.8244(14)	8.0856(13)	30.874(6)
α (°)	90	106.389(10)	90	90	90
β (°)	95.345(16)	102.151(9)	105.668(12)	92.234(14)	90.20(3)
γ (°)	90	100.772(9)	90	90	90
<i>V</i> (Å ³)	1241.5(4)	1180.3(3)	1452.5(5)	837.7(2)	1689.6(5)
<i>Z</i>	4	1	4	2	4
Reflections collected	4153	7070	3404	4170	5075
Unique reflections	1301	4356	1375	4170	2951
<i>R</i> _{int}	0.0716	0.0234	0.1602	0.0000	0.1016
<i>R</i> ₁ (<i>I</i> > 2σ(<i>I</i>))	0.0383	0.0432	0.0532	0.0601	0.0829
w <i>R</i> ₂ (all data)	0.0970	0.1272	0.1255	0.1666	0.2445

	6	7	8	9	10
Formula			C ₁₂ H ₂₀ CuN ₂ O ₁₁	C ₁₂ H ₂₀ N ₂ O ₁₁ Zn	C ₁₂ H ₂₀ CdN ₂ O ₁₁
<i>M_r</i>			431.84	433.67	480.70
Crystal system	Monoclinic	Monoclinic	Monoclinic	Orthorhombic	Orthorhombic
Space group			<i>P2/c</i>	<i>C222₁</i>	<i>C222₁</i>
<i>T</i> (K)	180(2)	180(2)	180(2)	180(2)	180(2)
<i>a</i> (Å)	15.2970(25)	15.3163(22)	15.211(3)	6.8874(7)	6.9402(7)
<i>b</i> (Å)	6.9180(12)	6.9200(12)	6.8469(14)	7.6896(8)	7.9330(7)
<i>c</i> (Å)	7.9090(18)	7.8249(19)	8.1434(16)	29.879(5)	29.988(4)
α (°)	90	90	90	90	90
β (°)	90.200(14)	90.198(13)	92.16(3)	90	90
γ (°)	90	90	90	90	90
<i>V</i> (Å ³)			847.5(3)	1582.5(3)	1651.0(3)
<i>Z</i>			2	4	4
Reflections collected			4578	2949	3396
Unique reflections			4578	1589	1545
<i>R</i> _{int}			0.0000	0.0251	0.0391
<i>R</i> ₁ (<i>I</i> > 2σ(<i>I</i>))			0.0741	0.0226	0.0295
w <i>R</i> ₂ (all data)			0.2099	0.0514	0.0590

**Scheme 2** The H₂IBG ligand possessing a hypothetical *btsta* conformation.

different conformations that this type of ligand can adopt which results from the flexible character of the arms of this organic molecule. This flexibility has been shown to lead to different conformations in previous examples,^{6d} and the nomenclature also simplifies the crystal structure description. For this purpose, we take into account (a) the positions of the two carbonyl groups of the two amides (*syn–anti*),¹² (b) the conformation of the amide (*trans–cis*) and (c) the position of the aliphatic (*R*₂, Scheme 1) residues *below* or *above* the plane of the aromatic ring. Thus, starting from the left to right (Scheme 2) an abbreviation such as *btsta* (*below, trans, syn, trans, above*) corresponds to a hypothetical conformation where the first glycine group is

below (*b*) the plane of the aromatic ring, the first amide group is *trans* (*t*), the carbonyl groups are in a *syn*-form (*s*), the second amide group is *trans* (*t*) and the second glycine group is above (*a*) the plane of the aromatic ring (Scheme 2).

Crystal structures description

H₂IBG (**1**) has a 2-fold rotation symmetry and consequently the torsion angles of its two halves are equal but with opposite signs. The two glycine residues are characterized by the torsion angles (C1C2N1C3) and (O2C1C2N1), the values of which are close to those found in the polyglycine II structure (61.6° and 155.5°, respectively).¹³ The molecular conformation is also characterized by the N1C3C4C7 torsion angle of 150.70 (13)°, which clearly deviates from 180°. Thus, a displacement of the planar amide group out of the plane of the benzene ring (29.5°) is produced. Adopting the nomenclature described above the conformation of the ligand can be described as *atstb*. As expected, compound **1** is extended to three dimensions through two strong hydrogen bonds; the first contains the nitrogen atom (N1) of the amide group and the oxygen atom (O3) of the amide group and the second contains the oxygen atom of the carboxylic

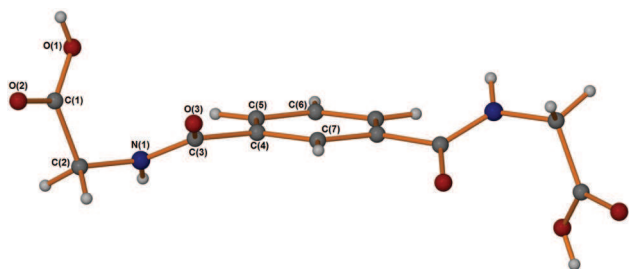


Fig. 1 Crystal structure of **1** possessing an *atstb* conformation.

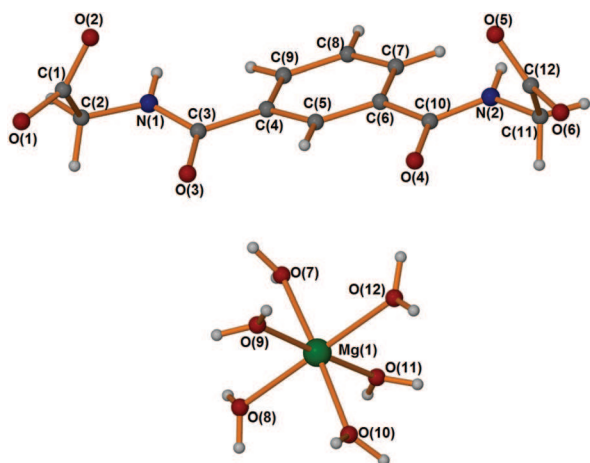


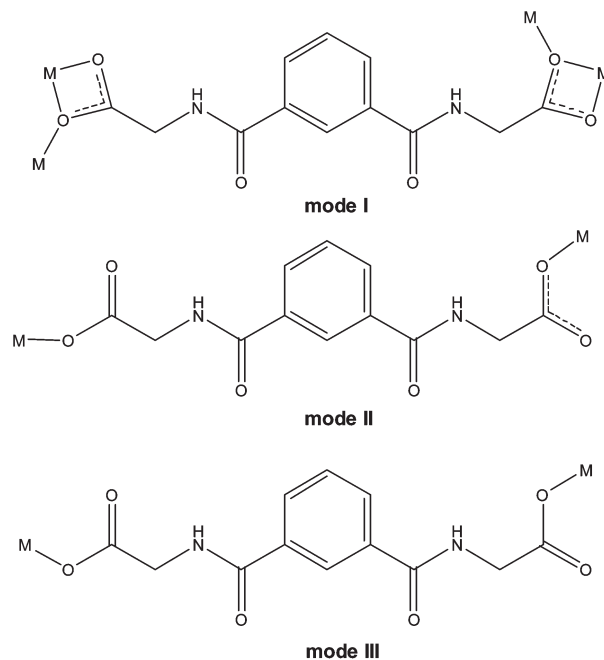
Fig. 2 The asymmetric unit of **2**. Mg green, O red, N blue, C grey. Lattice water molecules are omitted for clarity.

group (O1) and the oxygen atoms of the carbonyl group (O2). It is worth noting that no stacking interaction¹⁴ can be found in the crystal structure of **1** (Fig. 1).

The asymmetric unit of compound **2** consists of one Mg^{II}, one doubly deprotonated IBG organic dianion, six aqua ligands and 5.5 lattice water molecules. Surprisingly, the ligand is not coordinated to the Mg metal ion and interestingly the organic moiety adopts an *atsta* conformation (Fig. 2).

Before describing the crystal structures of compounds **3–10**, we note that upon ligand coordination to the metal centres the CH₂NHCO(*m*-C₆H₄)CONHCH₂ residue is flattened. In compounds **3–10**, the ligand coordinates to the metal centres through three different coordination modes which are depicted in Scheme 3.

The crystal structure of **3** (Fig. 3) reveals one dimensional (1D) Ca^{II} chains which are linked by IBG ligands into an infinite two dimensional (2D) network. The asymmetric unit of compound **3** comprises a half Ca^{II} centre, half a ligand and one ligated water molecule. Each Ca^{II} centre has a coordination number 8 with a geometry not close really to that described by ideal polyhedra such as a dodecahedron or a square antiprism.^{15a} The geometry of Ca^{II} in **3** is very close to that of Ca(NO₃)₂(MeOH)₄,^{15b} and the best fit is to a dodecahedron in which the bidentate ligands occupy an edge in opposite trapezoids. Each Ca^{II} centre is ligated to two chelate carboxylates, two water molecules and two bridging oxygen atoms belonging to two different carboxylates (Fig. 3 upper). Interestingly, the



Scheme 3 The three coordination modes of IBG found in **3–10**.

ligand adopts an *atsta* conformation, similar to that one observed in **2**, while the two carboxylate groups show as chelate-bridging modes (mode I, Scheme 3). There are two different metal–metal distances; the short Ca^{II}...Ca^{II} distance is 4.049(4) Å and each pair of adjacent Ca^{II} centres in the chain is bridged by a chelate-bridging carboxylate, with the chains propagating parallel to the *a* axis in the crystal (Fig. 3). The chains are further linked by IBG ligands (Ca^{II}...Ca^{II} distances 10.539 Å, 13.272 Å, 15.157 Å) parallel to the *b* axis forming an infinite 2D pattern (Fig. 3 centre), the topology of which gives a **sql** net.¹⁶ Moreover, the adjacent 2D grids are themselves connected by medium strength stacking interactions between the aryl rings of the IBG ligands to form a supramolecular 3D structure. The distances between the centroids of the aromatic rings are 3.428(3) Å, 3.563(3) Å and 4.081(3) Å, with projection distances of 3.318(2) and 3.321(2) Å and offsets from the vertical of 0.860 Å and 1.292 Å, respectively.¹⁴ The solvent-accessible volume has been calculated using Platon to be 5.2% of the unit cell (Fig. 3 lower).

Similarly to **3**, compound **4** consists of Sr^{II} chains linked through the IBG ligand to a 2D layer. The asymmetric unit contains a half Sr^{II} centre, half an IBG ligand, one and half ligated and one lattice water molecules. In **4**, Sr(1) is ligated to nine oxygen atoms, forming a polyhedron which can be best described as a tricapped trigonal prism.^{15a} In contrast to **2** and **3**, the ligand adopts a *btsta* conformation, while the two carboxylate groups show chelate-bridging (mode I, Scheme 3). There are two different metal–metal distances; the short Sr^{II}...Sr^{II} distance is 4.044(3) Å and each pair of adjacent Sr^{II} centres in the chain is bridged by a chelate-bridging carboxylate, with the chains propagating parallel to the *c* axis in the crystal (Fig. 4 upper). The chains are further linked by IBG ligands (Sr^{II}...Sr^{II} distances 15.246, 15.925, 17.533 Å) forming an infinite 2D grid parallel to the *a0c* plane. As for **3**, the topological evaluation of this net results in a **sql** topology.¹⁶ However, due to the different

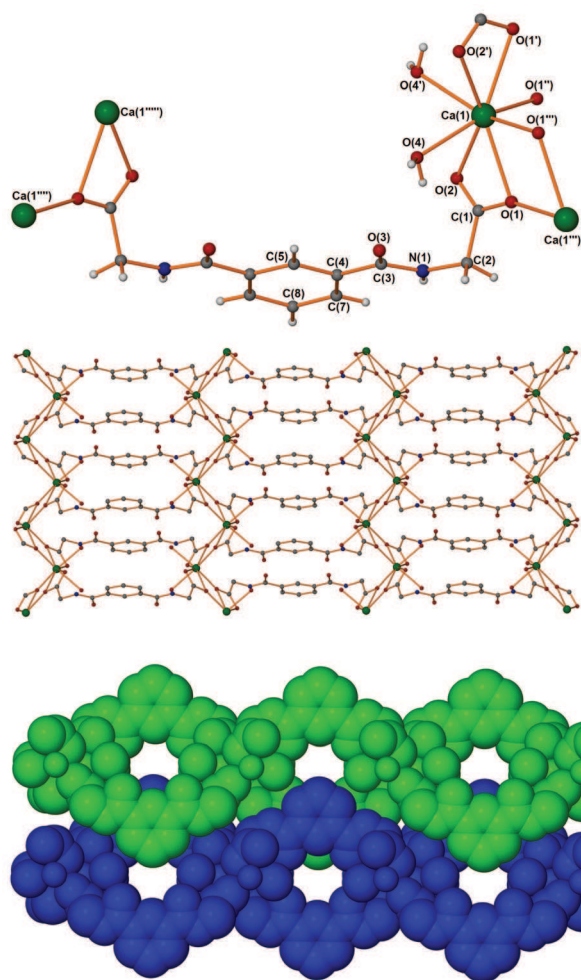


Fig. 3 (upper) The asymmetric unit of **3**. Ca green, O red, N blue, C grey. Lattice water molecules are omitted for clarity. (middle) A projection of the 2D network. (lower) A space filling diagram along the *a* axis indicating the small pores.

coordination environment of the metal centre, there is a difference in the stacking interactions motif. In **4**, the distance between the centroids of the aromatic rings is 4.081(3) Å, with a projection distance of 3.4489(19) Å and a high offset of 2.181 Å, indicating a weak stacking interaction (Fig. 4 lower).¹⁴

X-Ray single-crystal analysis reveals that **5** is composed of 1-D chains. The structure comprises a Mn^{II} centre, one IBG ligand, four ligated and two lattice water molecules, forming zig-zag [Mn(IBG)(H₂O)₄]_n 1D chains running along the *c* direction. Each Mn^{II} centre is situated in the center of a slightly distorted octahedron and ligated to four water molecules and to two oxygen atoms of two different carboxylates. All the Mn–O bonds are different and their length varies from 2.140(10) to 2.241(11) Å. The angle O(2)–Mn(1)–O(6) at 92.5(4)° exhibits a *cis* configuration of the two different IBG ligands. A similar coordination behavior was observed in the compound [Mn(TBG)(H₂O)₄]_n·2(H₂O), where TBG is the terephthaloylbisglycinate dianion.^{6c} In contrast to **2–4** the ligand adopts an *atstb* conformation and possesses the coordination mode II depicted in Scheme 3. A detailed study of the bond lengths and distances

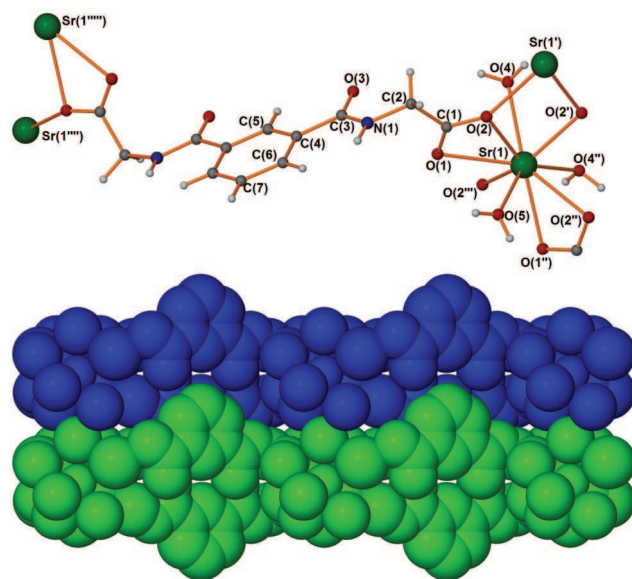


Fig. 4 (up) The asymmetric unit of **4**. Sr green, O red, N blue, C grey. Lattice water molecules are omitted for clarity. (down) A sphere packing diagram along the *c* axis indicating the difference in the packing diagram of **3**.

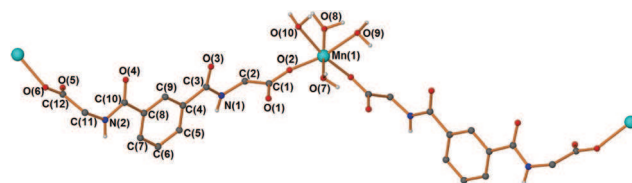


Fig. 5 The asymmetric unit of **5**. Mn light blue, O red, N blue, C grey. Lattice water molecules are omitted for clarity.

indicates that the two carboxylates behave differently; the first retains the single and double bond character with C(1)–O(1) and C(1)–O(2) being 1.228(18) and 1.285(18) Å respectively, while in the second a delocalization of the carboxylate group occurs with the C(12)–O(5) and C(12)–O(6) bonds being 1.25(2) and 1.253(19) Å, respectively (Fig. 5).

A combination of single crystal and powder diffraction measurements established that compounds **6–8** are isostructural (Table 1 and Fig. S3–S5†). Compounds **6** and **7** consistently gave crystals of rather poor quality; therefore their structures could not be refined. However, we were able to identify their unit cell (Table 1) and by recording their powder patterns (Fig. S4 and S5†) we identified that they are isostructural with compound **8** (Fig. 6).

X-Ray single-crystal analysis reveals that **8** is composed of 2-D layers. The asymmetric unit comprises a half Cu^{II} centre, half an IBG ligand, one and half ligated and one lattice water molecules. Each Cu^{II} centre is coordinated, in a rather regular octahedron to two oxygen atoms belonging to two monodentate carboxylates of two different IBG ligands, two bridging and two terminal water molecules, in *trans* positions. The bridging water molecules occupy the axial positions of the octahedron and their bond distances of 2.298(2) Å indicate large Jahn–Teller distortion. The ligand adopts an *atstb* conformation similar to **5** while

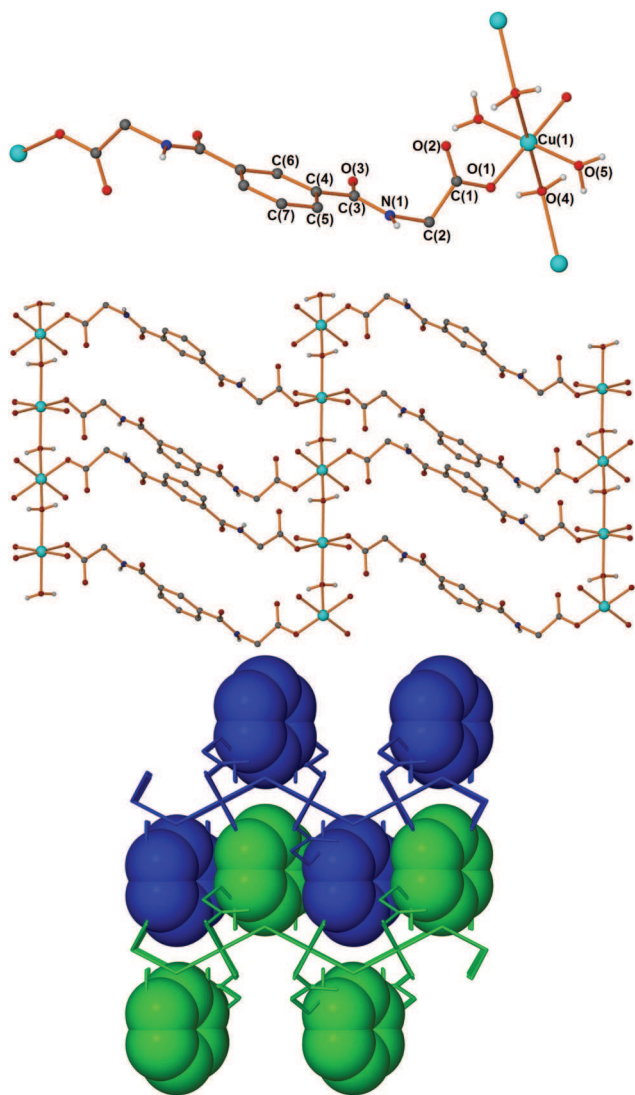


Fig. 6 (upper) The asymmetric unit of **8**. Cu light blue, O red, N blue, C grey. Lattice water molecules are omitted for clarity. (middle) A projection of the 2D network. (lower) A sphere packing diagram along the *a* axis indicating the interaction of the aromatic rings of different layers.

the X-ray structure shows that the ligand adopts the coordination mode III which is depicted in Scheme 3. The structure of **8** is constructed from 1D chains interlinked through bridging water and IBG groups into a 2D structure. The structure propagates along the *c* axis through the water bridge with a $\text{Cu}^{\text{II}} \cdots \text{Cu}^{\text{II}}$ distance of 4.072 Å, a value which is very close to previously reported examples,^{6a,17} while the IBG bridges propagate alternately parallel to the *ao**c* plane ($\text{Cu}^{\text{II}} \cdots \text{Cu}^{\text{II}}$ 15.598 Å). As for **3** and **4**, the topological evaluation of this net results in a **sql** topology.¹⁶ It is worth noting that the stacking interactions motif presented in **8** is similar to that found in **4**, indicating a weak strength stacking interaction.¹⁴ In **8**, the distance between the centroids of the aromatic rings is 4.101(3) Å, with a projection distance of 3.468(2) Å and a high offset of 2.190 Å.

Single crystal diffraction studies showed that compounds **9** and **10** are isostructural; thus only compound **9** will be further described. Compound **9** is composed of 1D $[\text{Zn}(\text{IBG})(\text{H}_2\text{O})_3]_n$

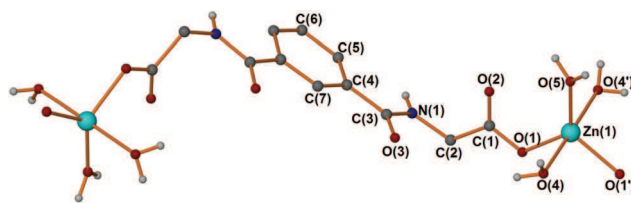


Fig. 7 The asymmetric unit of **9**. Zn light blue, O red, N blue, C grey. Lattice water molecules are omitted for clarity.

right handed helical chains running along the *c* direction (Fig. 7 upper). The refined Flack parameter of $-0.002(13)$ for **9** and $0.02(4)$ for **10** shows that the crystals examined have the same handedness throughout its structure, rather than being racemically-twinned with different domains containing right and left handed helices. Within a batch of crystals there will be comparable amounts of crystals showing either a right or left handed enantiomer.¹⁸ The Zn(1) atom and water oxygen O(5) lie on a two-fold axis and the IBG ligand lies about an inversion centre. Each Zn^{II} centre in **9** has a trigonal bipyramidal environment, coordination number 5, with one terminal water molecule and two oxygens belonging to two monodentate carboxylates of two different IBG ligands in the equatorial plane, while two terminal water molecules occupy the axial positions. Analysis of the shape determining angles using the approach of Addison, Reedijk *et al.*¹⁹ yields a value for the trigonality index, τ , of 0.85 for **9** suggesting trigonal bipyramidal geometry about Zn in both compounds ($\tau = 0$ and 1 for perfect square planar and trigonal bipyramidal geometries respectively). As for **8**, the ligand adopts an *atstb* conformation and shows a bis-monodentate coordination mode which is depicted in Scheme 3 (mode III). In addition, the $\text{Zn}^{\text{II}} \cdots \text{Zn}^{\text{II}}$ separation within the helical chain for **9** is 15.179 Å.

IR studies

The IR spectra of compounds **2–10** are consistent with what can be expected from the crystallographic studies. All the spectra show a very strong band in the region of $3340\text{--}3400\text{ cm}^{-1}$ indicating protonation of the nitrogen atom of the amide group, while the peaks around 1640 cm^{-1} indicate that the carbonyl group of the amide is not coordinated. The absence of any peak in the region of 1710 cm^{-1} and the existence of peaks around 1580 cm^{-1} indicate that the carboxylic groups are deprotonated. In Table 2 are depicted some characteristic bands of all compounds, including the potassium salt of the ligand (**1K**), in order to assign the coordination mode of the carboxylate group according to the literature.²⁰ The difference (Δ) of the asymmetric $\nu(\text{CO}_2)_{\text{as}}$ and symmetric $\nu(\text{CO}_2)_{\text{s}}$ bands of **1K** is 173 cm^{-1} , thus as anticipated for compounds **5–10** which show monodentate mode, Δ is higher than that of **1K** (Table 2). Interestingly, the difference in the values 177 cm^{-1} and 192 cm^{-1} found for **8** and **9** (Table 2) can be attributed to the slight difference in the bond distance of the carbonyl group of the carboxylate (1.237(7) in **8** and 1.229(3) in **9**) which indicates that the carbonyl group of the carboxylate in **9** has greater double bond character than in **8**. The Δ values of compounds **3** and **4** (chelate bridging mode, mode I, Scheme 3) are close to those of **1K**, while the Δ value of the ionic compound **2** is higher than in **1K**.

Table 2 Diagnostic IR bands of compounds **1–10** and the potassium salt of the ligand (**1K**)

Compound	$\nu(\text{NH})_{\text{-CONH}}$	$\nu(\text{CO}_2)_{\text{as}}$	$\nu(\text{C=O})_{\text{-CONH}}$	$\nu(\text{CO}_2)_{\text{s}}$	Δ (cm ⁻¹)
1	3287	1713	1643	1320	
1K	3356	1583	1638	1410	173
2	3324	1578	1636	1398	180
3	3398	1573	1633	1396	177
4	3402	1576	1646	1400	176
5	3333	1580	1634	1395	185
6	3350	1582	1651	1406	176
7	3343	1584	1653	1408	176
8	3364	1584	1654	1407	177
9	3348	1589	1630	1397	192
10	3348	1589	1630	1397	192

Table 3 ¹H and ¹³C NMR chemical shifts

	1	1Na	3	7	10
H _(OH)	12.08	—	—	—	—
H _(NH)	8.97	8.64	8.58	8.62	8.58
H _(CH2)	3.95, 3.96	3.95	3.90, 3.91	3.85	3.89, 3.90
C _(CH2)	41.24	43.23, 43.34	43.77, 43.89	43.95	43.75, 43.87
(C=O) _{amide}	166.02	169.75, 169.82	169.66, 169.72	169.94	169.73
(C=O) _{carb}	171.20	175.71	176.59	175.09	176.74

NMR studies

In order to investigate the solution behavior of the aforementioned compounds, NMR spectra were also recorded at pH 5 and in an M(II):ligand molar ratio 1 : 1. The ¹H- and ¹³C-NMR chemical shifts of the sodium salt of the ligand (**1Na**) and the compounds (**3**, **7**, **10**) were recorded in D₂O solution and the ligand in DMSO solution (Table 3).

The downfield chemical shift for NH in the ¹H-NMR spectrum of the ligand indicates that this H-atom is involved in H-bonding. The crystal structure of H₂IBG (**1**) shows the presence of an intermolecular H-bond between the NH group and the carbonyl O-atom of the amide group of another molecule. For compounds, **1Na**, **3**, **7** and **10**, the absence of any peak in the area of 12 ppm in the ¹H-NMR spectra indicates the deprotonation of the carboxylic group. The downfield chemical shift for NH in the ¹H-NMR spectrum of **1Na**, **3**, **7** and **10** indicates that this H-atom is involved in stronger H-bonding. In compounds **3**, **7** and **10** the H-atoms of the two methylene groups are shifted to lower chemical shifts due to the ligation of the ligand, while in the ¹³C-NMR spectrum the peaks of the methylene groups are shifted at higher values. The involvement of the carboxylic groups in bonding to the metal centres in **3**, **7** and **10** was also confirmed by the chemical shift of the carbon atom of the carboxylate groups which were shifted to higher values. In order to obtain a better understanding of the synthesis of those compounds a ¹¹³Cd NMR spectrum was recorded for compound **10** at pH 5. This (Fig. S7†) indicates that the ligand coordinates with the Cd centre in a chelated fashion; the geometry of each Cd centre in compound **10** is closely related to that of Cd(NO₃)₂·4H₂O.²¹ The crystalline solid which precipitated from the solution could be identified as compound **10** based on the powder XRD pattern.

Thermal studies

The powder XRD patterns of the bulk material of all compounds (Fig. S1–S6†) show that the previously crystallographically described compounds are the only products of these reactions. Thermogravimetric analysis (TGA) was carried out on compounds **3**, **6** and **10** (Fig. S8†). All water molecules were successfully removed from all compounds, as indicated by the lack of a mass loss around 100 °C. The decomposition of compounds **3**, **6** and **10** begins at 275 °C, 284 °C and 274 °C respectively, resulting in metal oxide as the final residue. The removal and reabsorption of the lattice and ligated water molecules of compounds **6–8** is successful (Fig. S4–S6†). Upon removal of the water molecules in **6**, each Co(II) centre adopts a tetrahedral geometry and when the rehydration procedure is followed it readopts an octahedral geometry (Fig. S9†).

Gas sorption studies

N₂ gas sorption experiments were carried out for compounds **3** and **8** with a Quantachrome Autosorb 1-MP. Prior to measurement the samples were outgassed at 95 °C overnight. The isotherms were run from partial pressure (p/p_0 where p_0 is the saturation pressure) from 10⁻⁵ to 1 p/p_0 (Fig. S10†). The N₂ cross section was assumed to be 0.162 nm². Specific surface area (SSA) was calculated according to the BET equation^{22a} and found to be 4.5 m² g⁻¹ for **3** and 12.0 m² g⁻¹ for **8**. The pore size distribution was determined following the NL-DFT method^{22b} using a slit pore geometry and N₂ sorption at 77 K on carbon with an NLDFIT equilibrium model resulting in 0.05 cm³ g⁻¹ for **3** and 0.09 cm³ g⁻¹ for **8** (pore volume calculated for a maximum pore size of 52 nm). Comparison of

the fitting error of different NL-DFT models, *i.e.* slit, cylindrical or a mixture of both, revealed that the pure slit geometry yielded the best agreement with the data.

Magnetic studies

Variable temperature dc magnetic susceptibility data were collected for compounds **6** and **7** in the temperature range 5–300 K under an applied field of 0.2 T. These are plotted as $\chi_M T$ versus T in Fig. 8 up. For **6**, the room temperature $\chi_M T$ value of 12.17 cm³ K mol^{−1} corresponds to two non-interacting Co^{II} ions with $S = 3/2$ and $g = 2.67$. Upon cooling the $\chi_M T$ value decreases to a minimum value of 0.59 cm³ K mol^{−1} at 5 K. Given the presence of octahedral Co^{II} ions with a ⁴T_{1g} ground term that splits into a doublet ground-state at low temperature when in a distorted environment due to spin–orbit coupling,²³ it is very laborious, extremely difficult and risky to apply an exact theoretical model for fitting the magnetic susceptibility data.²⁴ In addition, it should be noted that Co(II) ions in octahedral symmetry may be treated as pseudo-“ $s_{\text{eff}} = 1/2$ ” systems at low temperature due to the splitting of the Kramers doublets. Nevertheless, evidence supporting the presence of dominant

antiferromagnetic interactions arises from a Curie–Weiss analysis of the high temperature (40–300 K) magnetic susceptibility data with $\theta = -43.8$ K (Fig. 8 down).

For compound **7**, the room temperature $\chi_M T$ value of 2.22 cm³ K mol^{−1} is slightly lower than the expected value of 2.35 cm³ K mol^{−1} for two non-interacting Ni^{II} ions (with $g = 2.17$). Upon cooling the value of $\chi_M T$ decreases to a minimum value of 0.03 cm³ K mol^{−1} at 5 K, suggesting the presence of a relatively strong antiferromagnetic interaction. We were able to simulate the magnetic susceptibility data successfully using a $1 - J$ model and Hamiltonian (1) that assumes one exchange interaction between neighboring Ni^{II} centres by using the program MAGPACK²⁵ and employing the Hamiltonian in eqn (1).

$$\hat{H} = -2J(\hat{S}_1 \cdot \hat{S}_2) \quad (1)$$

This afforded the parameters $J = -15.25$ cm^{−1} and $g = 2.18$. The antiferromagnetic nature of J may be attributed to the large Ni–O_{water}–Ni angle found in **7**.

Theoretical studies. Theoretical studies of the “free-standing” H₂IBG and IBG^{2−} molecules

First we optimized the molecular geometries of the “free-standing” H₂IBG (**1**) ligand and its deprotonated dianionic conjugate base IBG^{2−} at the PBE0/6-311+G(d,p) level of theory. The equilibrium geometries along with selected structural parameters are shown in Fig. S11.†

It can be seen that contrary to 2-fold rotation symmetry of the crystal structure of the H₂IBG (**1**) ligand the DFT calculations predict a non-centrosymmetric structure for the “free-standing” molecule in the gas phase. One of the glycine residues is characterized by the torsion angles C4–C3–N2–C1 and O5–C4–C3–N2 of 170.6° and −1.9° respectively, while the other by the torsion angles C4–C3–N2–C1 and O5–C4–C3–N2 of −93.4° and −179.7° respectively. The molecule is also characterized by the O–C1–C7–O torsion angle of 4.5°. On the other hand, the two glycine residues in the IBG^{2−} ligand are characterized by the torsion angles C4–C3–N2–C1 and O5–C4–C3–N2 of 176.0° and 0.8° respectively, while the O–C1–C7–O torsion angle is 0.0°. The carboxylate moieties of the glycine residues in IBG^{2−} are found in the *syn* conformation with one of the oxygen atoms forming a hydrogen bond with the N–H hydrogen atom.

In the IR spectra of the H₂IBG species the diagnostic $\nu_{\text{str}}(\text{N–H})$, $\nu_{\text{as}}(\text{O=C=O})$, $\nu_{\text{str}}(\text{C=O})_{\text{amide}}$, $\nu_{\text{sym}}(\text{O=C=O})$ and $\nu_{\text{bend}}(\text{O=C=O})$ bands absorb at 3492–3523 cm^{−1}, 1773–1783 cm^{−1}, 1695–1712 cm^{−1}, 1329–1379 cm^{−1}, and 596–602 cm^{−1} respectively. In the IR spectrum of IBG^{2−} species the aforementioned diagnostic bands absorb at 3357–3358 cm^{−1}, 1654–1657 cm^{−1}, 1661–1669 cm^{−1}, 1335, 1336 cm^{−1} and 638–653 cm^{−1} respectively. The IR spectra of the “free-standing” H₂IBG and IBG^{2−} species are in good agreement with the experimentally obtained IR spectra of **1** and **1K** molecules.

A noteworthy point is the excellent agreement of the ¹H and ¹³C NMR chemical shifts (δ , ppm) calculated at the GIAO-PBE0/6-311+G(d,p) level listed in Fig. S12† (compare the values given in Table 3 with the calculated ones).

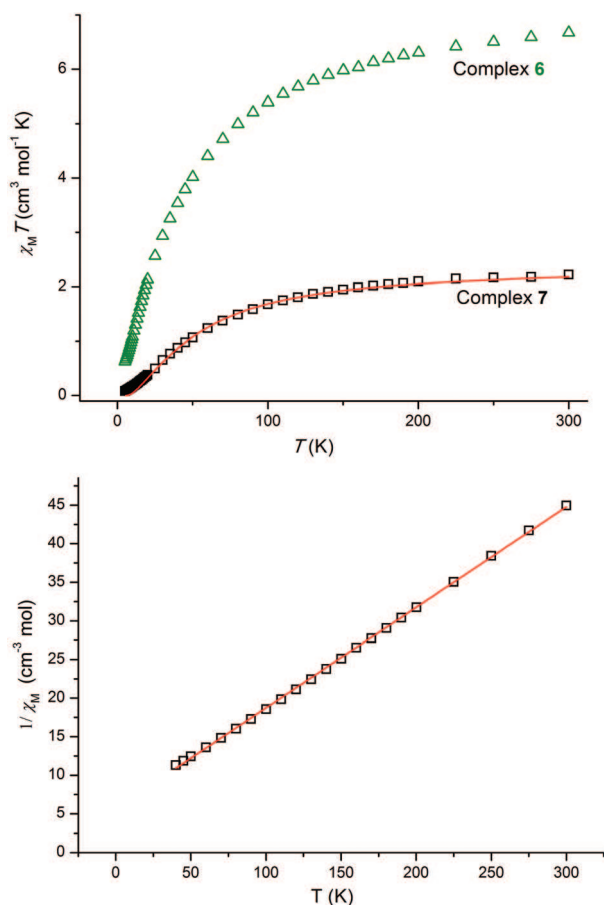


Fig. 8 (up) Plot of $\chi_M T$ vs. T for complexes **6** (green triangles) and **7** (black squares). The solid line represents a fit of the data in the temperature range 5–300 K (see text for details) (down) Curie–Weiss plot for complex **6** for the 40–300 K range.

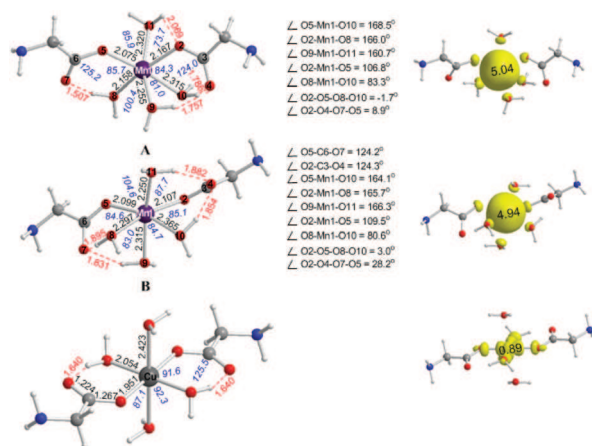


Fig. 9 Equilibrium geometries of the $\text{Mn}(\text{glycine})_2(\text{H}_2\text{O})_4$ and $\text{Cu}(\text{glycine})_2(\text{H}_2\text{O})_4$ complexes calculated at the DSD-PBEP86/Def2-TZVP level.

Theoretical studies of the model $\text{Mn}(\text{glycine})_2(\text{H}_2\text{O})_4$ and $\text{Cu}(\text{glycine})_2(\text{H}_2\text{O})_4$ complexes

To explain the preferred *syn* and *anti* configurations of the carbonyl groups of the two *trans* coordinated IBG ligands in the $[\text{Mn}(\text{IBG})_2(\text{H}_2\text{O})_4]_n$ (**5**) and $[\text{Cu}(\text{IBG})(\mu\text{-H}_2\text{O})(\text{H}_2\text{O})_2]_n$ (**8**) complexes respectively, we performed DFT calculations on the model $\text{Mn}(\text{glycine})_2(\text{H}_2\text{O})_4$ and $\text{Cu}(\text{glycine})_2(\text{H}_2\text{O})_4$ complexes. The equilibrium geometries of the $\text{Mn}(\text{glycine})_2(\text{H}_2\text{O})_4$ and $\text{Cu}(\text{glycine})_2(\text{H}_2\text{O})_4$ complexes calculated at the DSD-PBEP86/Def2-TZVP level of theory are shown in Fig. 9. The 3D plots of the total spin density are also shown in Fig. 9. DSD-PBEP86 is a recently developed functional that includes spin-component scaled MP2 and dispersion corrections.^{10a}

Perusal of Fig. 9 reveals that for the $\text{Mn}(\text{glycine})_2(\text{H}_2\text{O})_4$ complex two different low energy structures are obtained at the DSD-PBEP86/Def2-TZVP level depending on the starting geometry chosen. Structure **A** results from a starting geometry resembling the crystal structure of **5**, while structure **B** results from a starting geometry involving the two coordinated glycine ligands with their carbonyl groups in *anti* configuration. Structure **B** is slightly more stable (by 0.8 kcal mol⁻¹) than structure **A**. Both structures are non-centrosymmetric with the two carbonyl groups of the coordinated glycine ligands adopting the *syn* configuration closely resembling the crystal structure of **5**. All the Mn–O bonds are different with the bond lengths found in the range 2.075–2.365 in excellent agreement with the Mn–O bond lengths in the crystal structure of **5**. As in the case of complex **5** the two carboxylato moieties have different structural parameters, the first retains the double C=O and single C–O bond character with the C(6)–O(7) and C(6)–O(5) bond lengths in **A** (**B**) being 1.245(1.240) Å and 1.272(1.277) Å respectively, while in the second carboxylato group both C–O bonds acquire a partially double bond character with the C(3)–O(4) and C(3)–O(2) bond lengths in **A**(**B**) being 1.255(1.258) Å and 1.264(1.261) Å respectively.

It is noteworthy that four hydrogen bonds are present in structures **A** and **B** stabilizing the complexes. In a structure involving the *trans* coordinated glycine ligands with their carbonyl groups

adopting the *anti* configuration three hydrogen bonds are formed and this could be the reason for the preferred *syn* configuration of the carbonyl groups of the coordinated glycine ligands. The hydrogen bonds formed in the $\text{Mn}(\text{glycine})_2(\text{H}_2\text{O})_4$ and $\text{Cu}(\text{glycine})_2(\text{H}_2\text{O})_4$ complexes are clearly shown in the 3D plots of the reduced density gradient (RDG) shown in Fig. S13.†

The optimized geometry of the $\text{Cu}(\text{glycine})_2(\text{H}_2\text{O})_4$ complex corresponds to a rather regular centro-symmetric octahedron with large Jahn–Teller distortion. This structure closely resembles the crystal structure of complex **8**. Two of the coordinated water molecules occupy the axial positions having Cu–O bond lengths of 2.423 Å, the other two occupy *trans* equatorial positions with Cu–O bond lengths of 2.054 Å. The two glycine ligands are coordinated to the Cu^{II} metal centre in a monodentate fashion, their carbonyl groups adopting the *anti* configuration. The coordinated carboxylato groups retain the single C–O and double C=O bond character with bond lengths of 1.267 Å and 1.224 Å respectively. All attempts to locate on the potential energy surfaces (PES) the structure involving the two glycine ligands having their carbonyl groups in *syn* configuration starting from such geometry were unsuccessful due to convergence problems for a variety of functionals and basis sets tested. Finally, it is worth noting that the spin density is almost totally located on the central Mn and Cu metal atoms (Fig. 9).

To unveil the reason for the preferred configurations of the coordinated glycine ligands in the $\text{Mn}(\text{glycine})_2(\text{H}_2\text{O})_4$ and $\text{Cu}(\text{glycine})_2(\text{H}_2\text{O})_4$ complexes we calculated the potential energy surfaces (PES) for the adiabatic rotation of one of the glycine ligands around the Mn–O and Cu–O bonds respectively (Fig. 10).

Perusal of Fig. 10 reveals that the PES of the $\text{Mn}(\text{glycine})_2(\text{H}_2\text{O})_4$ complex is characterized by three minima corresponding to structures with torsion angles φ of 30°, 140° and 220°. The global minimum corresponds to the structure with $\varphi = 220^\circ$ involving the two *trans* coordinated glycine ligands with the carbonyl groups in *syn* configuration closely resembling the structure of complex **5**. The lowest energy structure involving the two *trans* coordinated glycine ligands with the carbonyl groups in *anti* configuration corresponds to the structure with $\varphi = 30^\circ$ which is predicted to be 23.8 kcal mol⁻¹ higher in energy than the global minimum structure. Here it is noteworthy that in the global minimum structure four hydrogen bonds are formed while in the structure with $\varphi = 30^\circ$ only one hydrogen bond shown in Fig. 10 with an O...H distance of 1.625 Å is formed. The higher number of hydrogen bonds formed in the global minimum structure relative to the structure with $\varphi = 30^\circ$ should be the reason for stabilizing the observed structure with the two *trans* coordinated glycine ligands with the carbonyl groups preferring the *syn* configuration. Also, in the low energy structure occurring at $\varphi = 140^\circ$ which is found to be 21.1 kcal mol⁻¹ higher in energy than the global minimum structure one hydrogen bond is formed. The global maximum (saddle point at $\varphi = 80^\circ$) is found to be 85.9 kcal mol⁻¹ higher in energy than the global minimum. It is worth noting that the predicted high rotational barrier prohibits any free rotation of the glycine ligand and therefore only the global minimum structure would exist.

The PES for the adiabatic rotation of one of the glycine ligands around the Cu–O bond in the $\text{Cu}(\text{glycine})_2(\text{H}_2\text{O})_4$ complex (Fig. S12†) is characterized by four minima and four

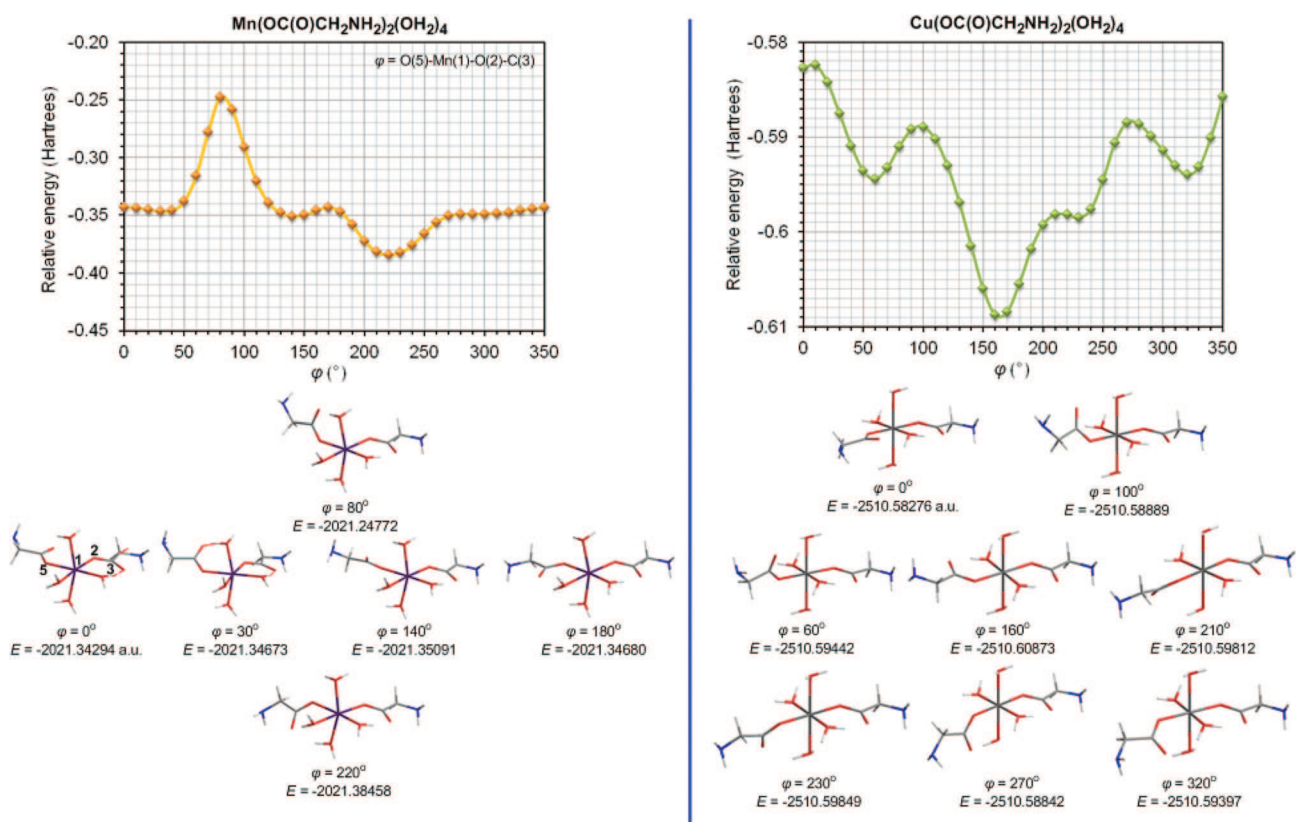


Fig. 10 Potential energy surface for the adiabatic rotation of one of the glycine ligands around the Mn–O and Cu–O bonds in the Mn(glycine)₂–(H₂O)₄ and Cu(glycine)₂(H₂O)₄ complexes respectively calculated at the DSD-PBEP86/Def2-TZVP level.

Table 4 Summary of herein reported results

Compound	Ligand conformation	Coordination mode	Coordination number	Coordination geometry	Dimension
2	<i>atsta</i>	None	6	Octahedron	0D
3	<i>atsta</i>	Chelate-bridging	8	Dodecahedron/square antiprism	2D
4	<i>btsta</i>	Chelate-bridging	9	Tricapped trigonal prism	2D
5	<i>atstb</i>	Monodentate	6	<i>cis</i> -Octahedron	1D
6	<i>atstb</i>	Monodentate	6	<i>trans</i> -Octahedron	2D
7	<i>atstb</i>	Monodentate	6	<i>trans</i> -Octahedron	2D
8	<i>atstb</i>	Monodentate	6	<i>trans</i> -Octahedron	2D
9	<i>atstb</i>	Monodentate	5	Trigonal bipyramidal	1D
10	<i>atstb</i>	Monodentate	5	Trigonal bipyramidal	1D

saddle points. The global minimum corresponds to the structure with $\varphi = 160^\circ$ involving the two *trans* coordinated glycine ligands with the carbonyl groups in *anti* configuration closely resembling the structure of complex **8**. The structure involving the two *trans* coordinated glycine ligands with the carbonyl groups in *syn* configuration corresponds to the structure with $\varphi = 10^\circ$ which is predicted to be the global maximum 15.6 kcal mol^{−1} higher in energy than the global minimum structure. It is clear that the global minimum structure is the preferred structure for the Cu(glycine)₂(H₂O)₄ complex rather than the structure with $\varphi = 10^\circ$ involving the two *trans* coordinated glycine ligands with the carbonyl groups in *syn* configuration. However, the relatively low rotational barrier of 15.6 kcal mol^{−1} allows rotation of the glycine ligands. Therefore low energy structures of the Cu(glycine)₂(H₂O)₄ complex corresponding to

minima at 60°, 210° and 320° could also be isolated. In this case it can be noted that there are two hydrogen bonds in the global minimum structure but only one in the global maximum structure, thus explaining the preferred *anti* configuration of the carbonyl groups of the two *trans* coordinated glycine ligands in the Cu(glycine)₂(H₂O)₄ complex in line with the experimentally determined structure of complex **8**.

Discussion

The results presented herein are summarized in Table 4. In the present study the coordination abilities of H₂IBG along with alkaline earth, transition metal elements, Zn(II) and Cd(II) were investigated. The different coordination behaviour of the ligand

observed in compounds **2**, **3** and **4** can be attributed to the different radii of the alkaline earth element. In compound **2** the ligand is isolated as a simple anion; this may be attributed to the fact that the radius of Mg(II) (coordination number 6) is rather small to accommodate the ligand and therefore is coordinated by six water molecules. In contrast, compounds **3** and **4** are 2D coordination polymers; the ligand shows similar coordination bis-chelating-bridging behaviour but different conformations, while Ca(II) and Sr(II) have coordination numbers 8 and 9 in **3** and **4**, respectively. A further increase in the radius of the alkaline earth by using Ba(II) (ligand conformation *btsta*, coordination number 9, geometry capped square antiprism, two different coordination modes; chelating-bridging and bidentate) does not increase the dimensionality of the final motif which is also a 2D layer structure motif although the structure is not reported here due to the poor quality of the crystals.

The ligand shows similar coordination mode (bis-monodentate) and conformation in compounds **5–10**, however there are basic differences in the shape of the final motif. A comparison with our previous studies with H₂TBG^{6a,c} (where R₁ = *p*-C₆H₄ and R₂ = CH₂, Scheme 1) along with a literature survey for the coordination abilities of hippuric acid²⁶ (where R₁ = C₆H₅, R₂ = CH₂, Scheme 1), a ligand which can be considered as the “parent” of H₂TBG and H₂IBG, shows that there is a systematic preference of ligation to the 3d transition, Zn(II) and Cd(II) metal elements. When Fe(II), Co(II), Ni(II) or Cu(II) metal centres are ligated to the aforementioned ligands, then each metal centre adopts a *trans*-octahedron geometry, while the axial positions of the metal centre are occupied by bridging water molecules. In contrast, when Mn(II) is ligated to this type of ligand a *cis* octahedral geometry is adopted. Theoretical studies were carried out for compounds **5** and **8** indicating that the difference in the coordination geometry of the metal centres in **5** and **8** is the result of the different number of hydrogen bonds formed within the crystal structures. Finally, Zn(II) and Cd(II) prefer a trigonal pyramidal geometry (coordination number 5) which is in agreement with previous results.^{6c}

A comparison of the present findings and our previous results^{6a,c} indicates that the change of the position of the (CONHCH₂COO) unit on the aromatic scaffold from *para* (where R₁ = *p*-C₆H₄, R₂ = CH₂, Scheme 1) to *meta* (where R₁ = *m*-C₆H₄, R₂ = CH₂, Scheme 1) prevents interpenetration. However the dimensionality of the final motif is decreased resulting in low-porosity compounds as confirmed by the adsorption studies. Magnetic studies carried out for compounds **6** and **7** support the presence of dominant antiferromagnetic interactions.

Moreover, from the crystal engineering point of view, it is worth mentioning that a comparison of the molecular formulas, the coordination behaviour of the ligand, and the coordination geometry of the metal centres in compounds **4** to **10** indicates that these results can be best described by the term pseudopolymorph.²⁷

Conclusions

A systematic investigation of the coordination chemistry of H₂IBG with different metal centres has been performed. We

have presented a detailed study of the coordination abilities of H₂IBG towards alkaline earth, 3d transition, Zn(II) and Cd(II) metal elements. It appears that apart from the coordination number of the metal centre, there are several factors affecting the network dimensionality for the room temperature reactions. Having gained these insights into the coordination behaviour of this ligand, our following efforts will be focused on increasing the dimensionality and porosity of the system using pillars such as 4,4-bipyridine.

Acknowledgements

The authors would like to thank Sven Stahl from the Institute of Nanotechnology at the Karlsruhe Institute of Technology for performing the elemental analysis, thermogravimetric analysis, NMR measurements and differential thermal analysis experiments.

Notes and references

- (a) C. Janiak and J. L. Vieth, *New J. Chem.*, 2010, **34**, 2366; (b) W. L. Leong and J. J. Vittal, *Chem. Rev.*, 2011, **111**, 688; (c) C. P. Li and M. Du, *Chem. Commun.*, 2011, **47**, 5958.
- A. Manton, L. Massüger, P. Rabu, C. Palivan, L. B. McCusker and A. Taubert, *J. Am. Chem. Soc.*, 2008, **130**, 2517.
- R. Ganguly, B. Sreenivasulu and J. J. Vittal, *Coord. Chem. Rev.*, 2008, **252**, 1027; C.-D. Wu, A. Hu, L. Zhang and W. Lin, *J. Am. Chem. Soc.*, 2005, **127**, 8940.
- (a) S. Blasco, M. I. Burguete, M. P. Clares, E. García-España, J. Escorihuela and S. V. Luis, *Inorg. Chem.*, 2010, **49**, 7841; (b) V. Martí-Centelles, D. K. Kumar, A. J. P. White, S. V. Luis and R. Vilar, *CrystEngComm*, 2011, **13**, 6997; (c) J. Becerril, M. Bolte, M. I. Burguete, J. Escorihuela, F. Galindo and S. V. Luis, *CrystEngComm*, 2010, **12**, 1722; (d) I. Alfonso, M. Bolte, M. Bru, M. I. Burguete, S. V. Luis and J. Rubio, *J. Am. Chem. Soc.*, 2008, **130**, 6137; (e) M. Bru, I. Alfonso, M. I. Burguete and S. V. Luis, *Angew. Chem., Int. Ed.*, 2006, **45**, 6155.
- (a) H.-T. Zhang and X.-Z. You, *Acta Crystallogr., Sect. E: Struct. Rep. Online*, 2005, **61**, m1163; (b) J. Duan, B. Zheng, J. Bai, Q. Zhang and C. Zuo, *Inorg. Chim. Acta*, 2010, **363**, 3172; (c) B. Wissler, A.-C. Chamayou, R. Miller, W. Scherer and C. Janiak, *CrystEngComm*, 2008, **10**, 461; (d) T. Min, B. Zheng, J. Bai, R. Sun, Y. Li and Z. Zhang, *CrystEngComm*, 2010, **12**, 70; (e) R. Sun, Y. Z. Li, J. Bai and Y. Pan, *Cryst. Growth Des.*, 2007, **7**, 890; (f) R. Sun, S. N. Wang, H. Xing, J. Bai, Y. Z. Li, Y. Pan and X. Z. You, *Inorg. Chem.*, 2007, **46**, 8451.
- (a) G. E. Kostakis, L. Casella, N. Hadjiliadis, E. Monzani, N. Kourkoulis and J. C. Plakatouras, *Chem. Commun.*, 2005, 3859; (b) J. G. Servetas, G. E. Kostakis, M. Haukka, T. Bakas and J. C. Plakatouras, *Polyhedron*, 2009, **28**, 33221; (c) G. E. Kostakis, L. Casella, A. K. Boudalis, E. Monzani and J. C. Plakatouras, *New J. Chem.*, 2011, **35**, 1060; (d) C. N. Morrison, A. K. Powell and G. E. Kostakis, *Cryst. Growth Des.*, 2011, **11**, 3653; (e) K. F. Konidaris, A. K. Powell and G. E. Kostakis, *CrystEngComm*, 2011, **13**, 5872; (f) K. F. Konidaris, C. N. Morrison, J. G. Servetas, M. Haukka, Y. Lan, A. K. Powell, J. C. Plakatouras and G. E. Kostakis, *CrystEngComm*, 2012, **14**, 1842; (g) K. F. Konidaris, A. C. Tsipis and G. E. Kostakis, *ChemPlusChem*, 2012, **77**, 354; (h) V. N. Dokorou, A. K. Powell and G. E. Kostakis, *Polyhedron*, 2012, DOI: 10.1016/j.poly.2012.08.032.
- (a) K. C. Mondal, G. E. Kostakis, Y. Lan, C. E. Anson and A. K. Powell, *Inorg. Chem.*, 2009, **48**, 9205; (b) S. Mukherjee, Y. Lan, G. E. Kostakis, R. Clérac, C. E. Anson and A. K. Powell, *Cryst. Growth Des.*, 2009, **9**, 577; (c) Z.-Y. Du, H.-R. Wen, C.-M. Liu, Y.-H. Sun, Y.-B. Lu and Y.-R. Xie, *Cryst. Growth Des.*, 2010, **10**, 3721; (d) L. Tian, Z.-J. Zhang, A. Yu, W. Shi, Z. Chen and P. Cheng, *Cryst. Growth Des.*, 2010, **10**, 3847; (e) M.-H. Zeng, Y.-L. Zhou, M.-C. Wu, H.-L. Sun and M. Du, *Inorg. Chem.*, 2010, **49**, 6436.
- (a) C. A. Williams, A. J. Blake, C. Wilson, P. Hubberstey and M. Schröder, *Cryst. Growth Des.*, 2008, **8**, 911; (b) D. W. Lee, V. Jo and K. M. Ok, *Cryst. Growth Des.*, 2011, **11**, 2698; (c) R. P. Davies,

- R. J. Less, P. D. Lickiss and A. J. P. White, *Dalton Trans.*, 2007, 2528;
- (d) I. Senkovska and S. Kaskel, *Eur. J. Inorg. Chem.*, 2006, 4564.
- 9 M. J. Frisch, G. W. Trucks, H. B. Schlegel, G. E. Scuseria, M. A. Robb, J. R. Cheeseman, J. A. Montgomery, Jr., T. Vreven, K. N. Kudin, J. C. Burant, J. M. Millam, S. S. Iyengar, J. Tomasi, V. Barone, B. Mennucci, M. Cossi, G. Scalmani, N. Rega, G. A. Petersson, H. Nakatsuji, M. Hada, M. Ehara, K. Toyota, R. Fukuda, J. Hasegawa, M. Ishida, T. Nakajima, Y. Honda, O. Kitao, H. Nakai, M. Klene, X. Li, J. E. Knox, H. P. Hratchian, J. B. Cross, V. Bakken, C. Adamo, J. Jaramillo, R. Gomperts, R. E. Stratmann, O. Yazyev, A. J. Austin, R. Cammi, C. Pomelli, J. W. Ochterski, P. Y. Ayala, K. Morokuma, G. A. Voth, P. Salvador, J. J. Dannenberg, V. G. Zakrzewski, S. Dapprich, A. D. Daniels, M. C. Strain, O. Farkas, D. K. Malick, A. D. Rabuck, K. Raghavachari, J. B. Foresman, J. V. Ortiz, Q. Cui, A. G. Baboul, S. Clifford, J. Cioslowski, B. B. Stefanov, G. Liu, A. Liashenko, P. Piskorz, I. Komaromi, R. L. Martin, D. J. Fox, T. Keith, M. A. Al-Laham, C. Y. Peng, A. Nanayakkara, M. Challacombe, P. M. W. Gill, B. Johnson, W. Chen, M. W. Wong, C. Gonzalez and J. A. Pople, Gaussian, Inc., Wallingford CT, 2004.
- 10 (a) S. Kozuch and J. M. L. Martin, *Phys. Chem. Chem. Phys.*, 2011, **14**, 20801; (b) F. Weigend and R. Ahlrichs, *Phys. Chem. Chem. Phys.*, 2005, **7**, 3297; (c) M. Ernzerhof and G. E. Scuseria, *J. Chem. Phys.*, 1999, **110**, 5029; (d) C. Adamo and V. Barone, *Chem. Phys. Lett.*, 1997, **274**, 242; (e) C. Adamo and V. Barone, *J. Chem. Phys.*, 1999, **110**, 6160; (f) C. Adamo, G. E. Scuseria and V. Barone, *J. Chem. Phys.*, 1999, **111**, 2889; (g) C. Adamo and V. Barone, *Theor. Chem. Acc.*, 2000, **105**, 169; (h) V. Vetter, C. Adamo and P. Maldivi, *Chem. Phys. Lett.*, 2000, **325**, 99; (i) H. B. Schlegel, *J. Comput. Chem.*, 1982, **3**, 214; (j) J. P. Merrick, D. Moran and L. Radom, *J. Phys. Chem. A*, 2007, **111**, 11683; (k) R. Ditchfield, *Mol. Phys.*, 1974, **27**, 789; (l) J. Gauss, *J. Chem. Phys.*, 1993, **99**, 3629; (m) T. Lu and F. Chen, *J. Comput. Chem.*, 2012, **33**, 580.
- 11 G. M. Sheldrick, *Acta Crystallogr. Sect. A: Fundam. Crystallogr.*, 2008, **64**, 112.
- 12 (a) R. Katoono, H. Kawai, K. Fujiwara and T. Suzuki, *Tetrahedron Lett.*, 2006, **47**, 1513; (b) H. Kawai, R. Katoono, K. Fujiwara, T. Tsuji and T. Suzuki, *Chem.-Eur. J.*, 2005, **11**, 815; (c) M. S. Betson, J. Clayden, H. K. Lam and M. Helliwell, *Angew. Chem., Int. Ed.*, 2005, **44**, 1241; (d) K. Yamaguchi, G. Matsumura, H. Kagechika, I. Azumaya, Y. Ito, A. Itai and K. Shudo, *J. Am. Chem. Soc.*, 1991, **113**, 5474; (e) S. J. Brooks, P. A. Gale and M. E. Light, *CrystEngComm*, 2006, **8**, 877.
- 13 F. H. C. Crick and A. Rich, *Nature*, 1955, **176**, 780.
- 14 C. Janiak, *J. Chem. Soc., Dalton Trans.*, 2000, 3885.
- 15 (a) M. G. B. Drew, *Coord. Chem. Rev.*, 1977, **24**, 179; (b) A. Leclaire, *Acta Crystallogr. Sect. B: Struct. Crystallogr. Cryst. Chem.*, 1974, **30**, 2259.
- 16 V. A. Blatov, *IUCr CompComm Newsletter*, 2006, **7**, 4.
- 17 (a) E. V. Karpova, A. I. Boltalin, Y. M. Korenev and S. I. Troyanov, *Koord. Khim.(Russ.)(Coord.Chem.)*, 2000, **26**, 384; (b) I. Gautier-Luneau, D. Phanon, C. Duboc, D. Luneau and J.-L. Pierre, *Dalton Trans.*, 2005, 3795.
- 18 Z. Majeeed, K. C. Mondal, G. E. Kostakis, Y. Lan, C. E. Anson and A. K. Powell, *Chem. Commun.*, 2010, **46**, 2551.
- 19 A. W. Addison, T. N. Rao, J. Reedijk, J. V. Rijn and G. C. Verschoor, *J. Chem. Soc., Dalton Trans.*, 1984, 1349.
- 20 (a) G. B. Deacon and R. J. Phillips, *Coord. Chem. Rev.*, 1980, **33**, 227; (b) K. Nakamoto, in *Infrared and Raman Spectra of Inorganic and Coordination Compounds*, Wiley, New York, 4th edn, 1986, p. 234.
- 21 M. F. Summers, *Coord. Chem. Rev.*, 1988, **86**, 43.
- 22 (a) S. Brunauer, P. H. Emmett and E. Teller, *J. Am. Chem. Soc.*, 1938, **60**, 309; (b) S. Lowell, J. E. Shields, M. A. Thomas and M. Thommes, Springer Verlag, 2006, ISBN-13-978-1-4020-2303-3 (e-book), p. 347.
- 23 (a) R. L. Carlin, *Magnetochemistry*, Berlin, Springer-Verlag, 1986; (b) O. Kahn, *Molecular Magnetism*, New York, Wiley-VCH, 1993.
- 24 Representative references and ref. therein: (a) F. Klöwer, Y. Lan, J. Nehrkorn, O. Waldmann, C. E. Anson and A. K. Powell, *Chem.-Eur. J.*, 2009, **15**, 7413; (b) E. C. Yang, D. N. Hendrickson, W. Wernsdorfer, M. Nakano, L. N. Zakharov, R. D. Sommer, A. L. Rheingold, M. Ledezma-Gairaud and G. Christou, *J. Appl. Phys.*, 2002, **91**, 7382; (c) Y.-Z. Zhang, W. Wernsdorfer, F. Pan, Z.-M. Wang and S. Gao, *Chem. Commun.*, 2006, 3302; (d) O. Waldmann, M. Ruben, U. Ziener, P. Müller and J. M. Lehn, *Inorg. Chem.*, 2006, **45**, 6535; (e) H. Andres, J. M. Clemente-Juan, M. Aebersold, J. M. Güdel, E. Coronado, H. Büettner, G. Kearly, J. Melero and R. Burriel, *J. Am. Chem. Soc.*, 1999, **121**, 10028; (f) A. V. Palii, B. S. Tsukerblat, E. Coronado, J. M. Clemente-Juan and J. J. Borrás-Almenar, *Inorg. Chem.*, 2003, **42**, 2455; (g) L. Banci, A. Bencini, C. Benelli, D. Gatteschi and C. Zanchini, *Struct. Bonding*, 1982, **52**, 37; (h) R. Boča, *Struct. Bonding*, 2006, **117**, 1; (i) M. Moragues-Canovás, C. E. Talbot-Eeckelaers, L. Catala, F. Lloret, W. Wernsdorfer, E. K. Brechin and T. Mallah, *Inorg. Chem.*, 2006, **45**, 7038; (j) J. M. Clemente-Juan, E. Coronado, A. Gaita-Ariño, C. Giménez-Saiz, H.-U. Güdel, A. Sieber, R. Bircher and H. Mutua, *Inorg. Chem.*, 2005, **44**, 3389; (k) J. M. Clemente-Juan, E. Coronado, A. Forment-Aliaga, J. R. Galan-Mascaros, C. Gimenez-Saiz and C. J. Gomez-Garcia, *Inorg. Chem.*, 2004, **43**, 2689.
- 25 (a) J. J. Borrás-Almenar, J. M. Clemente-Juan, E. Coronado and B. S. Tsukerblat, *Inorg. Chem.*, 1999, **38**, 6081; (b) J. J. Borrás-Almenar, J. M. Clemente-Juan, E. Coronado and B. S. Tsukerblat, *Comput. Chem.*, 2001, **22**, 985.
- 26 (a) M. M. Morelock, M. L. Good, L. M. Trefonas, D. Karraker, L. Maleki, H. R. Eichelberger, R. Majeste and J. Dodge, *J. Am. Chem. Soc.*, 1979, **101**, 4858; (b) J. N. Brown and L. M. Trefonas, *Inorg. Chem.*, 1973, **12**, 1730; (c) M. M. Morelock, M. L. Good, L. M. Trefonas, R. Majeste and D. Karraker, *Inorg. Chem.*, 1982, **21**, 3044; (d) H. Grewe, M. R. Udupa and B. Krebs, *Inorg. Chim. Acta*, 1982, **63**, 119; (e) G. Battistuzzi, M. Borsari, L. Menabue, M. Saladini and M. Sola, *Inorg. Chem.*, 1996, **35**, 4239; (f) S. Natarajan, S. A. M. B. Dhas, J. Suresh and R. V. Krishnakumar, *Acta Crystallogr. Sect. E: Struct. Rep. Online*, 2007, **63**, m1408; (g) S. Natarajan, S. A. M. B. Dhas, J. Suresh and S. Athimoolam, *Acta Crystallogr. Sect. E: Struct. Rep. Online*, 2007, **63**, m1941.
- 27 (a) H. H. Monfared, A.-C. Chamayou, S. Khajeh and C. Janiak, *CrystEngComm*, 2010, **12**, 3526; (b) D. Kovala-Demertzi, J. Wiecek, J. C. Plakatouras and Z. Ciunik, *CrystEngComm*, 2008, **10**, 1291.